Available online at www.sciencedirect.com
ScienceDirect
Journal of Solid State Chemistry 180 (2007) 148–157
JOURNAL OF SOLID STATE CHEMISTRY
www.elsevier.com/locate/jssc

$EuBaFe_2O_{5+w}$: Valence mixing and charge ordering are two separate cooperative phenomena

P. Karen[a,*], K. Gustafsson[b], J. Lindén[b]

[a]*Department of Chemistry, University of Oslo, P.O. Box 1033 Blindern, N-0315 Oslo, Norway*
[b]*Department of Physics, Åbo Akademi, FI-20500 Turku, Finland*

Received 6 September 2006; received in revised form 19 September 2006; accepted 24 September 2006
Available online 10 October 2006

Abstract

Mixed-valence $EuBaFe_2O_{5+w}$ exhibits a robust Verwey-type transition. The trend in the volume change suggests a first-order transition up to the nonstoichiometry level of about $w = 0.25$. ^{57}Fe Mössbauer spectroscopy, differential scanning calorimetry and synchrotron X-ray powder diffraction are used to study the valence mixing and charge ordering in $EuBaFe_2O_{5+w}$ as a function of the nonstoichiometry parameter w. ^{151}Eu Mössbauer spectroscopy is used as a selective probe into the ferromagnetic valence-mixing coupling along c above the Verwey transition, and reveals that increasing w destroys this coupling in favor of a G-type magnetic order in parallel with the progressive removal of the valence-mixed iron states accounted for by ^{57}Fe Mössbauer spectroscopy. This removal proceeds according to a probability scheme of mixing between ferromagnetically coupled divalent and trivalent neighbor iron atoms along c across the R layer. In contrast, the concentration decrease of the orbital- and charge-ordered states in $EuBaFe_2O_{5+w}$ is found to be a linear function of w. Valence mixing and charge ordering are therefore two separate cooperative phenomena. The enthalpy of the Verwey-type transition between these two cooperative systems is a linear function of w, which suggests that it originates from the latent heat of freezing into the long-range ordered orbital- and charge-ordered state. The enthalpy becomes zero at the nonstoichiometry level of about $w = 0.25$.

PACS: 61.10.Nz; 61.18.Fs; 61.50.Ks; 82.60.Fa

Keywords: Oxygen nonstoichiometry versus charge ordering and valence mixing; Mixed valence; Iron perovskite oxides; ^{151}Eu and ^{57}Fe Mössbauer spectroscopy

1. Introduction

After the preceding article on charge ordering in $EuBaFe_2O_5$ [1], this paper deals with the effect of the oxygen nonstoichiometry on valence mixing and charge ordering in what is now expressed by the formula $EuBaFe_2O_{5+w}$. The $RBaFe_2O_{5+w}$ phases [2] of large trivalent rare-earth ions (R = Nd, Sm, Eu and Gd) are able to accommodate very high levels of oxygen nonstoichiometry [3,4]. Because the added oxygens are situated in the R layer, decreasing the size of R acts against this nonstoichiometry. On the other hand, decreasing the size makes it easier for the iron charges to order at sufficiently low temperatures [5]. The R = Eu phase appears to be around an optimum with respect to these two effects [5]. The added oxygens w destabilize both the iron valence mixing and charge (i.e., valence) ordering [3,4,6]. Whereas the concentration of $Fe^{2.5+}$ decreases progressively with increasing w according to a probability model [6] of competitive mixing between Fe^{3+} and the minority Fe^{2+} at room temperature, the behavior of the low-temperature charge-ordered states under the increasing nonstoichiometry has not been established.

The decrease of the valence mixing and ordering as a function of w in $EuBaFe_2O_{5+w}$ is evaluated in this study via both colligative and local approach. The former uses thermodynamic parameters such as T_V, ΔH, ΔS and ΔV obtained by differential scanning calorimetry (DSC) and synchrotron X-ray powder diffraction (SXPD), the latter

*Corresponding author. Fax: +47 228 554 41.
E-mail address: pavel.karen@kjemi.uio.no (P. Karen).

0022-4596/$ - see front matter © 2006 Elsevier Inc. All rights reserved.
doi:10.1016/j.jssc.2006.09.031

involves accounting for all present spin- and valence-states of iron with the help of ^{57}Fe Mössbauer spectra. The probability model of valence mixing is revisited in the light of the recently identified [7] ferromagnetic coupling along c between the mixing atoms. ^{151}Eu Mössbauer spectroscopy is used as a selective probe into this coupling as a function of w; something that would not be accessible by neutron diffraction owing to the high neutron absorption of Eu.

2. Experimental

Oxygen content control: The oxygen nonstoichiometry was controlled by high-temperature equilibration of a $EuBaFe_2O_{5+w}$ master sample [1] for 5–7 days in flowing $Ar-H_2-H_2O$ atmospheres, and subsequent quenching into streaming Ar (<2 ppm O_2, dried over a P_2O_5 desiccant). The nonstoichiometry characteristics for typical samples are listed in Table 1. All were single phase according to SXPD, and were stored under argon in order to prevent oxidation. As a precaution, a thin surface layer was removed before further characterizations. Oxygen contents were determined by cerimetric titrations [2].

Characterizations: SXPD data for $EuBaFe_2O_{5+w}$ were collected at 200 and 320 K using the BM1B powder diffractometer with a cryostat at ESRF Grenoble on samples sealed in glass capillaries (0.25 mm diameter) in steps of 0.002° 2θ. Rietveld refinements of the crystal structure data were done in the GSAS programme suite [8]. Short isothermal scans over Bragg reflections 200, 020, 004 of the double perovskite structure were performed across the main and premonitory Verwey-type transition upon heating. A liquid-nitrogen operated Perkin–Elmer Pyris 1 differential scanning calorimeter was used to register thermal flux curves upon heating (10 K/min) between 170 and 340 K [4]. ^{57}Fe and ^{151}Eu Mössbauer spectra were collected and evaluated as described in Ref. [1].

3. Results

3.1. Structural changes under increasing oxygen nonstoichiometry

Diffraction patterns for this series were not collected at a high-intensity beamline, and superstructure reflections for the $w = 0.007$ sample at 200 K were weak. Structural parameters were therefore refined consistently on the double-perovskite cell, and are listed in Tables 2 and 3. As done previously [3,4], insertion of the large oxygen atoms into the small O(4) site is modeled by a split Fe site.

There are two main indicators of the charge ordering in mixed-valence $EuBaFe_2O_{5+w}$: the superstructure Bragg peaks and the large orthorhombic distortion. While the superstructure vanishes already at low levels of w, the enhanced orthorhombic distortion, a consequence of ordering of the doubly occupied d_{xz} orbitals of divalent iron [9], persists up to about $w = 0.25$, with a residual distortion still apparent at $w = 0.333$ (Table 2). This remarkable difference can be explained by noting that the superstructure is associated with symmetry breaking by the O(3) and O(1) atoms. Each of these two atoms must shift coherently with their equivalent atoms in the neighboring unit cells. If these shifts were not coherent over a long range, that is not in one direction for all equivalent atoms, the superstructure would not appear. Once the added oxygens chop the coherently diffracting areas of the charge order into pieces, the direction of the shift may get reverted at the defects, and only the orthorhombic distortion remains to testify about the charge order. The thermal displacement parameters B_{iso} become accordingly increased.

Fig. 1 displays the volume, cell dimensions and orthorhombic distortion (on a background of the DSC peak) for a sample having w practically zero. Whereas no detectable volume change can be associated with the premonitory charge ordering at about 300 K, a significant volume change is observed at the main Verwey-type transition at 255 K. The onset of the charge ordering is manifested by a sudden increase in the orthorhombic distortion. Fig. 2 shows that the discontinuity in volume at T_V, defining the first order of the transition, persists into high levels of the oxygen nonstoichiometry.

3.2. Thermodynamic data

The ideal semi-integer valence 2.5+ of iron corresponds to the ideal formula $EuBaFe_2O_5$. This composition is associated with the largest entropy and volume change under the Verwey-type transition. As apparent from Fig. 3, the increasing oxygen nonstoichiometry interferes with the ordering of the two iron valences, and, by doing

Table 1
Nonstoichiometry control and characterizations (t in °C, p in bars) of main $EuBaFe_2O_{5+w}$ samples used for diffraction

w	a (Å)	b (Å)	c (Å)	Ar/H$_2$[a]	$\log_{10}(p_{H_2O})$	$\log_{10}(p_{O_2})$	t
0.007(1)	3.9571(5)	3.9385(5)	7.5995(13)	9.19(0)	−1.70	−15.81(1)	1000
0.063(2)	3.9568(5)	3.9397(6)	7.6112(13)	63.7(3)	−1.79	−14.39(1)	1000
0.149(2)	3.9439(4)	3.9439(4)	7.6112(11)	198(6)	−1.74	−13.28(4)	1000
0.224(1)	3.9421(3)	3.9421(3)	7.6663(9)	333(18)	−1.70	−12.75(6)	1000
0.333(1)	3.9381(3)	3.9381(3)	7.7008(10)	880(137)	−1.72	−11.92(15)	1000
0.415(1)	3.9355(4)	3.9355(4)	7.7216(11)	1788(42)	−1.65	−11.05(3)	1000

[a]By volume; standard deviations refer to variations over time.

Table 2
Rietveld refinement parameters for $EuBaFe_2O_{5+w}$ at 200 K within the double-perovskite cell; neglecting superstructure order

$w =$	0.007	0.063	0.149	0.224	0.333	0.415
R_{F^2}	0.0479	0.0315	0.0448	0.0447	0.0405	0.0598
N_{obs}	127	125	185	171	121	90
R_p	0.0492	0.0624	0.0677	0.0641	0.0498	0.0583
λ (Å)	0.50019	0.50019	0.50019	0.48572	0.50019	0.50086
Unit-cell parameters						
a (Å)	4.04014(1)	4.02796(2)	3.99644(1)	3.96899(5)	3.93765(1)	3.93032(1)
b (Å)	3.87095(1)	3.87704(2)	3.89407(1)	3.91359(5)	3.93253(1)	
c (Å)	7.58503(2)	7.59993(3)	7.63427(2)	7.65993(10)	7.69345(2)	7.71201(3)
Volume (Å^3)	118.624(1)	118.685(1)	118.808(1)	118.982(4)	119.133(1)	119.131(1)
Atom positions	*Pmmm*	*Pmmm*	*Pmmm*	*Pmmm*	*Pmmm*	*P4/mmm*
z(Fe)	0.2618(2)	0.2609(3)	0.2589(4)	0.2565(7)	0.2583(3)	0.2567(2)
z[O(2)]	0.3097(4)	0.3080(7)	0.3054(5)	0.3035(7)	0.2968(4)	0.2952(3)
z[O(3)]	0.3084(4)	0.3065(7)	0.3054(5)	0.3035(7)	0.2968(4)	n.a.
Displacement parameters $U_{iso} \times 100$ (Å^2)						
Eu,Ba	0.41(1)	0.56(1)	0.72(1)	0.87(2)	1.29(1)	0.41(1)
Fe	0.43(2)	0.45(3)	0.65(3)	0.55(3)	0.80(2)	0.71(2)
Oxygens	0.62(8)	0.62(10)	0.39(9)	1.66(10)	2.12(7)	0.40(5)
Bond distances (Å)						
Fe–O(1)	1.9857(16)	1.9825(25)	1.9763(32)	1.965(5)	1.9872(24)	1.9797(18)
Fe–O(2)	1.9693(7)	1.9714(10)	1.9792(9)	1.9897(14)	1.9885(5)	1.9874(4)
Fe–O(3)	2.0508(6)	2.0437(10)	2.0296(8)	2.0169(14)	1.9910(5)	n.a.

Pmmm: Eu $00\frac{1}{2}$, Ba 000, Fe $\frac{11}{22}z$ with fraction $1-w$, Fe′ $\frac{11}{22}0.25$ with fraction w. O(1) $\frac{11}{22}0$, [O(2) $\frac{1}{2}0z$, O(3) $0\frac{1}{2}z$] (z constrained equal), O(4) $\frac{111}{222}$ with fraction w. *P4/mmm*: the same as above, except that O(2) ≡ O(3). Except for $w = 0.007$ sample, $z[O(2)] = z[O(3)]$ was constrained.

Table 3
Structure refinement parameters for $EuBaFe_2O_{5+w}$ at 320 K

$w =$	0.007	0.063	0.149	0.224	0.333	0.415
R_{F^2}	0.0655	0.0555	0.0308	0.0435	0.0381	0.0501
N_{obs}	73	81	25	140	20	35
R_p	0.0586	0.0607	0.0600	0.0558	0.0711	0.0508
λ (Å)	0.50019	0.50019	0.50019	0.48572	0.50019	0.50019
Unit-cell parameters						
a (Å)	3.95597(2)	3.95231(2)	3.94439(2)	3.94217(1)	3.93876(2)	3.93586(1)
b (Å)	3.94145(2)	3.94319(2)				
c (Å)	7.60077(3)	7.61426(5)	7.64541(5)	7.66874(3)	7.70331(4)	7.72406(4)
Volume (Å^3)	118.513(1)	118.666(2)	118.949(2)	119.178(1)	119.508(2)	119.654(1)
Atom positions	*Pmmm*	*Pmmm*	*P4/mmm*	*P4/mmm*	*P4/mmm*	*P4/mmm*
z(Fe)	0.2639(2)	0.2623(3)	0.2604(3)	0.2598(3)	0.2594(7)	0.2573(4)
z[O(2)/O(3)]	0.3092(4)	0.3080(5)	0.3056(4)	0.3064(4)	0.3022(10)	0.2963(4)
Displacement parameters $U_{iso} \times 100$ (Å^2)						
Eu,Ba	0.92(2)	1.12(2)	1.49(5)	0.87(1)	4.96(5)	1.20(2)
Fe	0.90(3)	1.08(4)	1.21(5)	0.45(2)	4.26(8)	2.08(3)
Oxygens	1.27(10)	1.16(12)	1.79(17)	1.57(7)	8.25(21)	1.25(9)
Bond distances (Å)						
Fe–O(1)	2.0058(16)	1.9976(24)	1.9908(23)	1.9920(20)	1.999(5)	1.9876(29)
Fe–O(2)	2.0006(6)	2.0020(8)	2.0022(7)	2.0034(6)	1.9968(16)	1.9908(6)
Fe–O(3)	2.0077(6)	2.0065(8)	n.a.	n.a.	n.a.	n.a.

Pmmm: Eu $00\frac{1}{2}$, Ba 000, Fe $\frac{11}{22}z$ with fraction $1-w$, Fe′ $\frac{11}{22}0.25$ with fraction w, O(1) $\frac{11}{22}0$, [O(2) $\frac{1}{2}0z$, O(3) $0\frac{1}{2}z$] (z constrained equal), O(4) $\frac{111}{222}$ with fraction w. *P4/mmm*: the same as above, except that O(2) ≡ O(3).

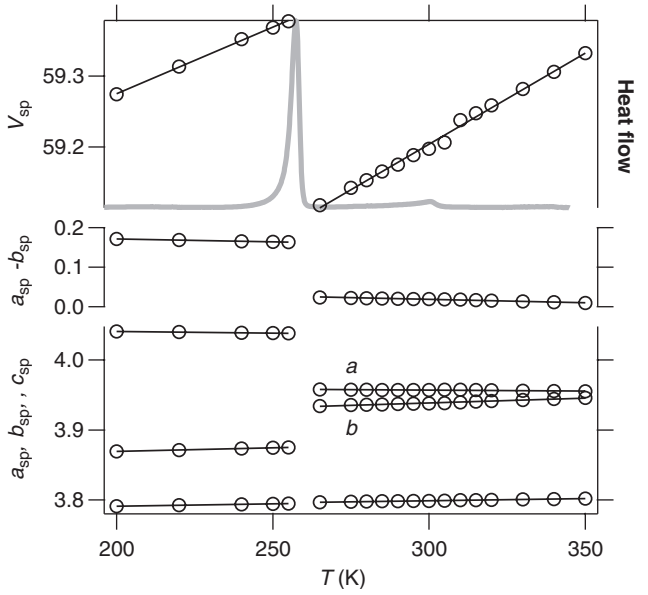

Fig. 1. Single-perovskite-type cell parameters (in Å) of $EuBaFe_2O_{4.992}$ as a function of temperature. (The volume discontinuity above the Verwey transition is spurious.)

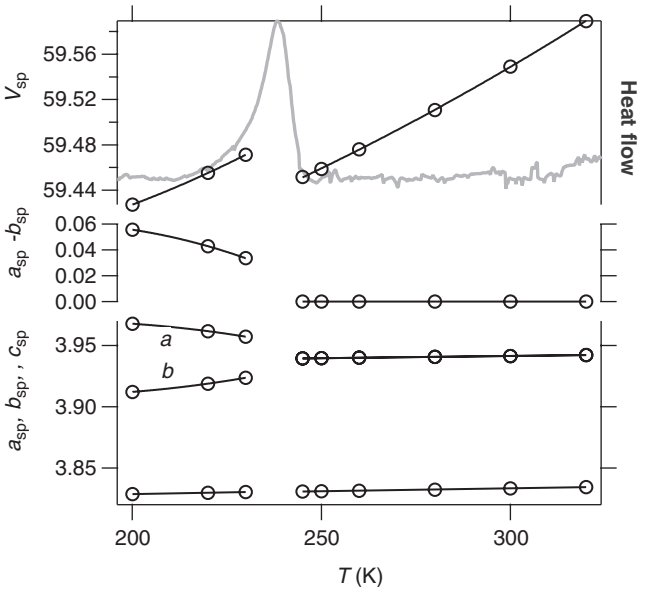

Fig. 2. Single-perovskite-type cell parameters (in Å) of $EuBaFe_2O_{5.224}$ as a function of temperature.

so, it decreases the thermal effect (latent heat) of the transition. Thermodynamic parameters derived from DSC (thermal data) and SXPD (molar volume data) are shown in Fig. 4 as a function of the nonstoichiometry parameter w. Extrapolation of the volume change at the main Verwey-type transition, ΔV, to zero shows that the discontinuity of the transition would disappear around $w = 0.26$. This value is close to the limit determined from extrapolations of the DSC-based transition entropies and enthalpies in Fig. 5.

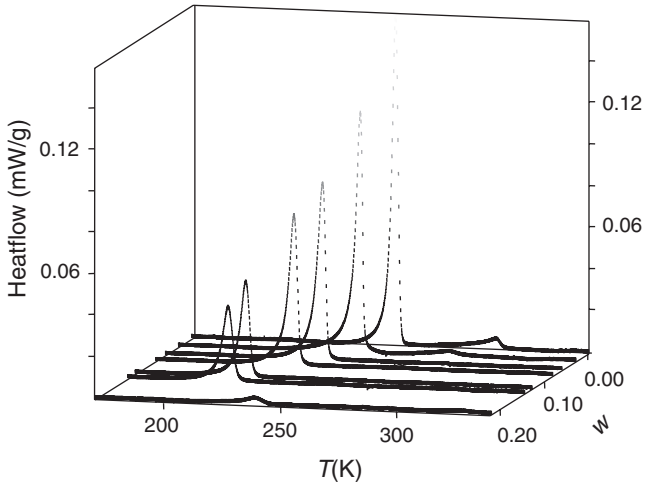

Fig. 3. DSC peaks for $EuBaFe_2O_{5+w}$ with $w = 0.003$, 0.033, 0.063, 0.085, 0.132, 0.149 and 0.224.

The plot in Fig. 5 is constructed following a procedure developed previously [4,5], which relates the Verwey transition enthalpy, entropy and T_V to the nonstoichiometry parameter w through the analogy with the freezing of an ideal solution. The solution is defined as that of the added oxygens w, represented by $EuBaFe_2O_6$ taken formally as a solute, with $EuBaFe_2O_5$ as a solvent. Starting with, say, a completely frozen solvent, every added oxygen (w) removes a certain fixed number of unit cells of the charge-ordered "ice" (that would melt discontinuously), and this causes a perfectly linear decrease in the "latent heat". Fig. 5 even implies what this number is, because the observed limit of $w \approx 0.25$ suggests that it is four single-perovskite-type cells (hence one unit cell of the charge-ordered type) that are removed from the charge-ordered "ice" by one added O(4) oxygen. With the transition enthalpy expressed as

$$\Delta H(w) = \Delta H(0)\left[1 - \frac{w}{w(0)}\right], \tag{1}$$

the composition dependence of the transition temperature, $T_V(w) = \Delta H(w)/\Delta S(w)$ follows from the analogy with depression of the freezing point for the above-defined ideal solution, derived from equating chemical potentials of the pure solvent in the "solid" and "liquid":

$$\frac{\Delta H(w)}{\Delta S(w)} = \frac{\Delta H(0)}{\Delta S(0) - R\ln(1-w)}. \tag{2}$$

The parameters $\Delta H(0)$, $\Delta S(0)$ and $w(0)$ are the fusion enthalpy and entropy of the pure solvent and the nonstoichiometry where the former two parameters become zero, respectively. Eqs. (1) and (2) have been simultaneously fitted by least squares to the experimental $\Delta H(w)$ and $\Delta S(w)$ values for the main Verwey transition in Fig. 5, yielding $\Delta H(0) = 1.984(46)\,\mathrm{kJ\,mol^{-1}}$, $\Delta S(0) = 7.794(48)\,\mathrm{J\,mol^{-1}\,K^{-1}}$ and $w(0) = 0.234(3)$.

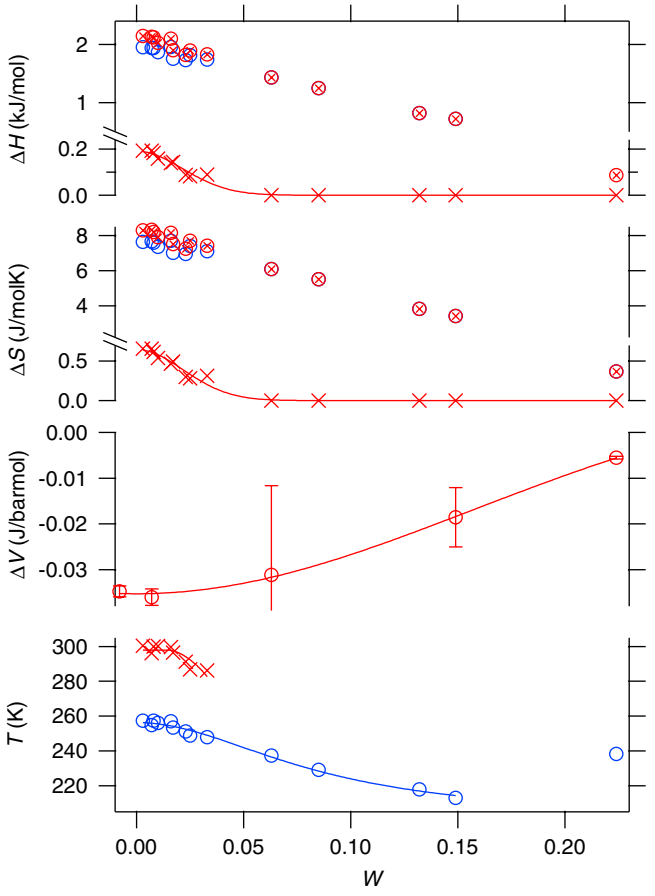

Fig. 4. Thermodynamic parameters of the charge-ordering transitions in $EuBaFe_2O_{5+w}$: premonitory (crosses), main transition (circles), the total of these (circles with crosses), estimated standard deviations are marked where available. The connecting lines are guides for the eye.

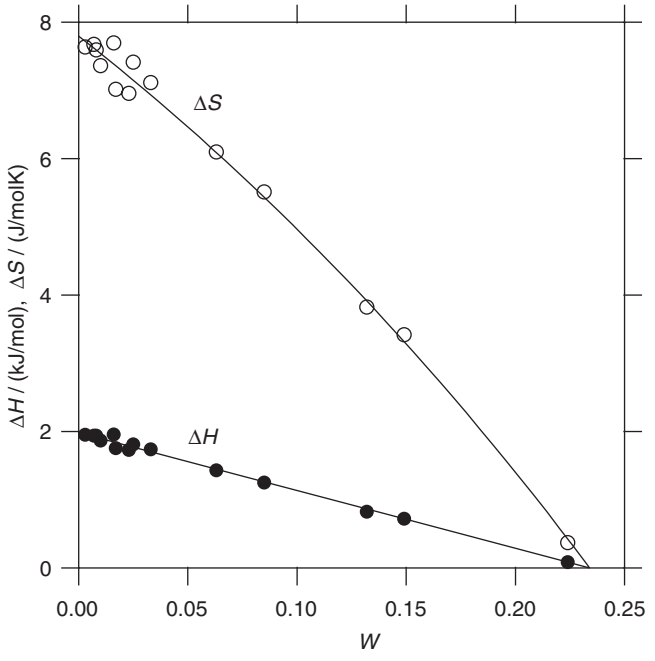

Fig. 5. Enthalpy and entropy of the main Verwey-type transition as a function of w; fitted according to the ideal-solution model of depression of the freezing point.

3.3. ^{57}Fe Mössbauer data

The effect of nonstoichiometry was studied both in the valence-mixed phase at 313 K and in the charge-ordered phase at 77 K by recording ^{57}Fe Mössbauer spectra of various $EuBaFe_2O_{5+w}$ samples. Fig. 6 illustrates that increasing w in the valence-mixed state increases concentration of the minority components $^{CN5}Fe^{3+}_{50\,T}$ and $^{CN5}Fe^{2+}_{25\,T}$, which correspond to di- and trivalent Fe atoms not participating in the valence mixing. A satellite component $^{CN5}Fe^{3+}_{40\,T,\,satel}$ appears; associated [6] with the local competition of the valence states to mix valences. The last component, Fe_{par}, is featureless, weak and is apparently associated with thermally induced paramagnetic state of iron in the sample. Although the spectra recorded above the premonitory transition become increasingly complicated upon increasing w, the fitting is eased by the fact that

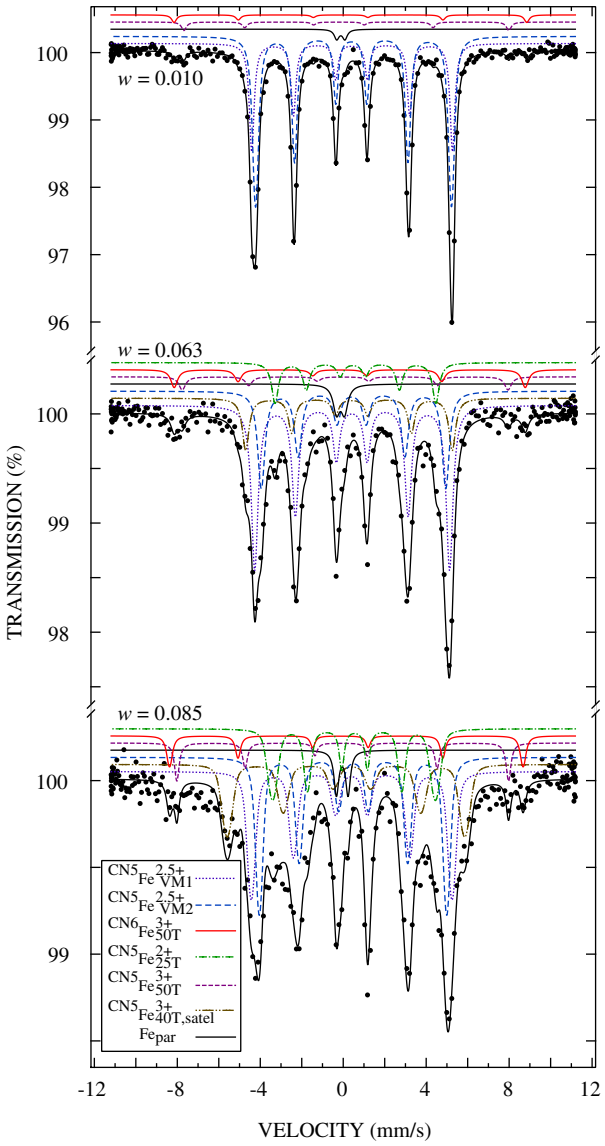

Fig. 6. ^{57}Fe Mössbauer spectra of $EuBaFe_2O_{5+w}$ at 313 K. Components used in the fitting are displayed above the data and identified in the legend.

the spectral components form distinct groups: two ~50 T components, the ~30 T valence-mixed component(s), the paramagnetic component, and the satellite of ~40 T evolving from non-mixing Fe^{3+} species.

Fig. 7 shows that increasing w in the charge-ordered state increases concentrations of those minority components that are present independently of temperature and hence were already observed at 313 K $^{CN5}Fe^{2+}_{25\,T}$ with isomer shift of ~1.0 mm/s, and $^{CN5}Fe^{3+}_{50\,T}$, both excluded from valence mixing/ordering for probability reasons, as well as the regular $^{CN6}Fe^{3+}_{50\,T}$.

3.4. ^{151}Eu Mössbauer data

The typical feature of the ^{151}Eu Mössbauer spectra of $EuBaFe_2O_{5+w}$, collected at 300 K, is narrowing of the total absorption peak as a function of increasing w (Fig. 8).

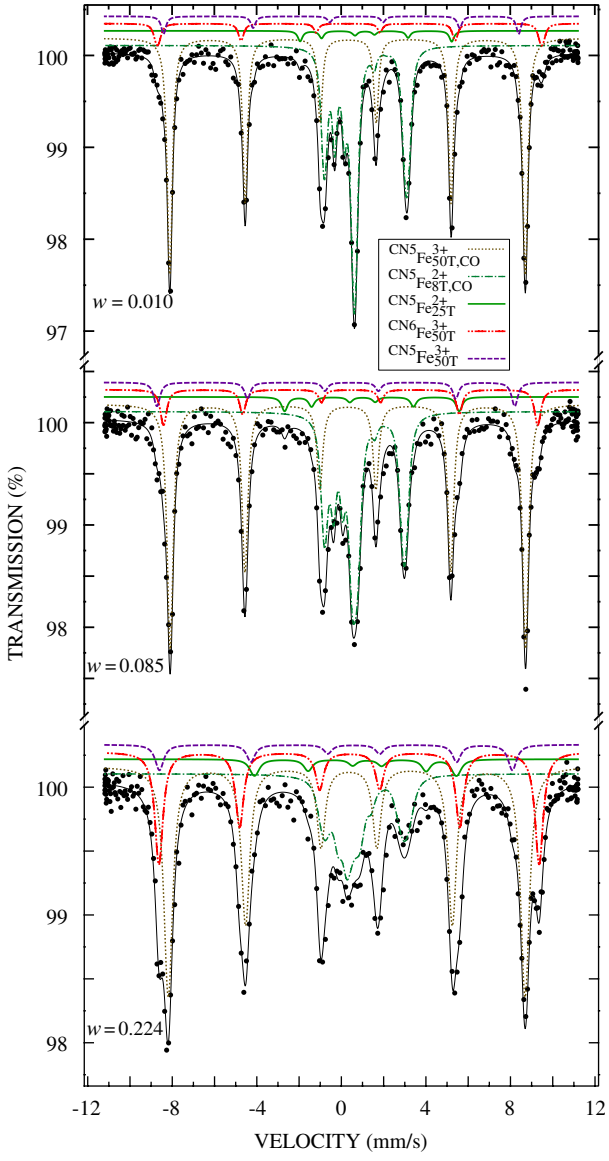

Fig. 7. ^{57}Fe Mössbauer spectra of $EuBaFe_2O_{5+w}$ at 77 K. Components used in the fitting are displayed above the data and identified in the legend.

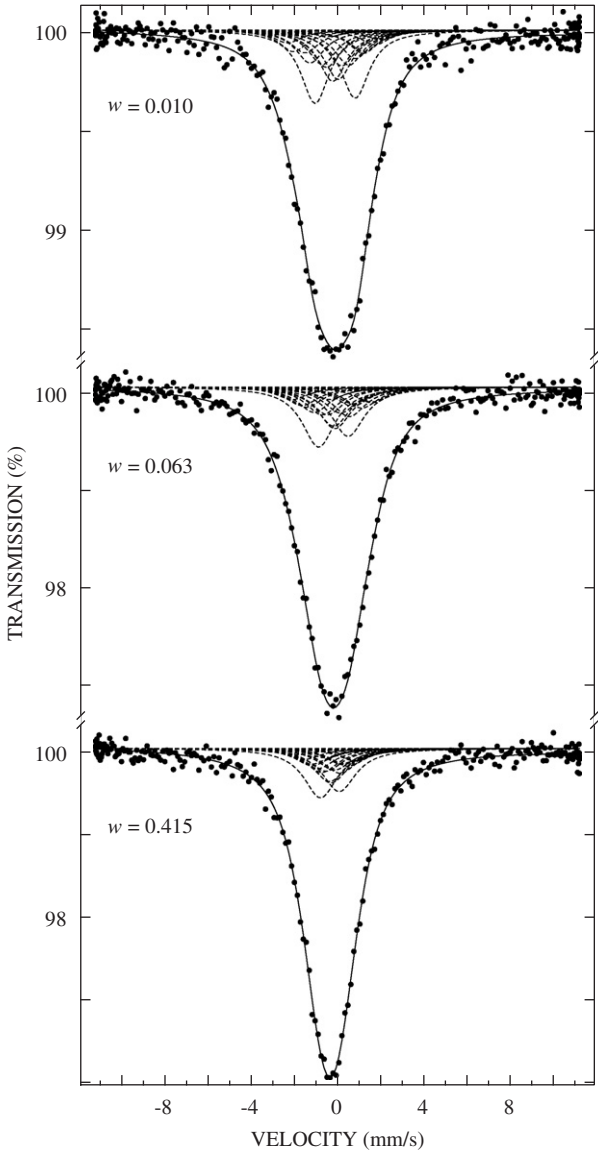

Fig. 8. ^{151}Eu Mössbauer spectra of $EuBaFe_2O_{5+w}$ recorded at 300 K.

As shown in the preceding article [1], the main origin of the non-Lorentzian shape of the $w = 0.010$ spectrum is the nonzero internal magnetic field (B) seen at the Eu nucleus, splitting the peak into many (48 in total) overlapping absorption states. Upon increasing w, both B and the electric field gradient V_{zz} decrease, which narrows and reshapes the total absorption peak. In Fig. 9, the main hyperfine parameters obtained from the least-squares fits are shown as a function of w. As will be illustrated in Section 4, the decrease in B as a function of w follows the decrease in concentration of the valence-mixed $Fe^{2.5+}$. The latter state is being replaced by a mixture of regular di- and trivalent iron atoms that would be expected to favor the G-type antiferromagnetic order, in which the magnetic moments seen at the Eu site cancel out.

Of other Mössbauer parameters, the isomer shift is also decreased by the oxygen loading, and this is seen in Fig. 8 as a shift of the total absorption peak towards negative

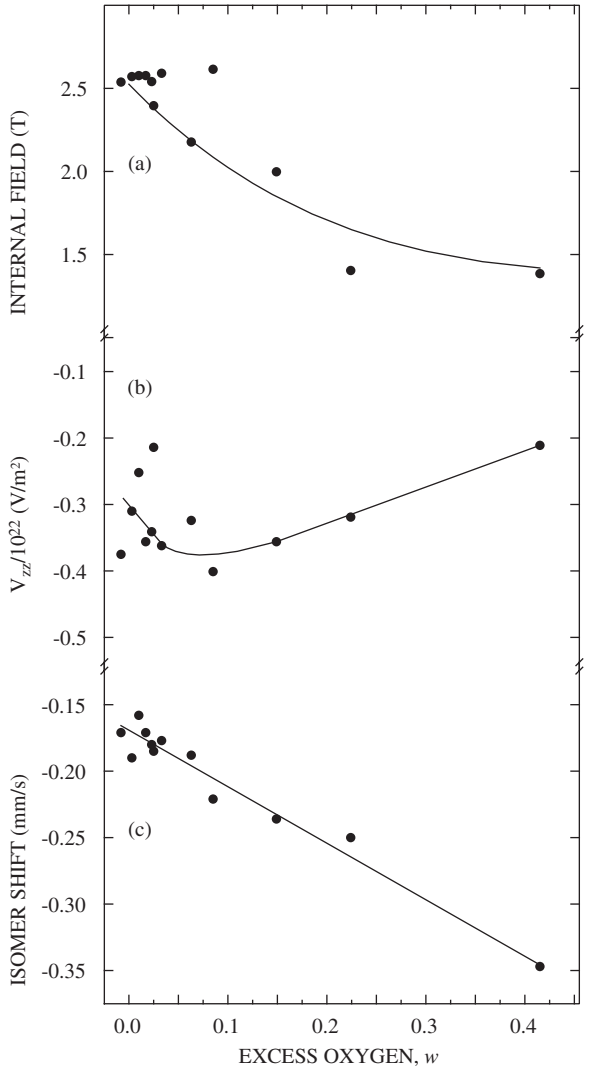

Fig. 9. Hyperfine ^{151}Eu Mössbauer parameters for $EuBaFe_2O_{5+w}$ at 300 K as a function of w: (a) internal magnetic field B, with a curve according to Eq. (3). (b) Main component of the electric field gradient, V_{zz}, with fitted curve as a guide for the eye. (c) Isomer shift with fitted line.

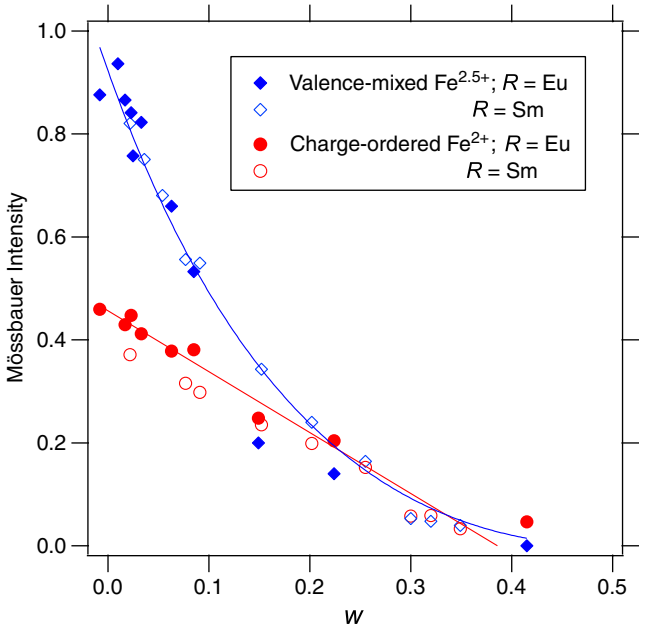

Fig. 10. Mössbauer-based fraction of iron atoms in valence-mixed state at 310 K (full diamonds; curve fitted by Eq. (3)) and fraction of divalent charge-ordered iron atoms at 77 K (bullets; line drawn as a guide for eye). Analogous data for $R = Sm$ from Ref. [6] are in open symbols.

velocities. The asymmetry parameter η (not shown in Fig. 9) increases from around 0.4 to 0.6 upon increasing w. The angles α and β that relate B and V_{zz} remain the same as reported [1] for the stoichiometric phase. The decrease in the absolute value of V_{zz} can be understood in terms of the anisotropic expansion, caused by increasing w, of the original c-axially compressed EuO_8 cube towards a regular EuO_{12} cuboctahedron (Table 3).

4. Discussion

4.1. Valence mixing under oxygen nonstoichiometry

The fraction of the valence-mixed iron, $x_{Fe^{2.5+}}$, is obtained from intensities of the ^{57}Fe Mössbauer components. Fig. 10 shows that this fraction decreases rapidly upon increasing w, and this is explained by the following model of valence mixing as electron sharing between divalent and trivalent iron, illustrated in Fig. 11: (1) the sharing occurs across the R layer along c, avoiding spin flip. (2) All minority Fe^{2+} (fraction $0.5 - w$) face five-coordinated Fe^{3+} across the R layer, owing to Coulombic minimization, and form a candidate valence-mixing pair. (3) Electron sharing will not work if, on either side along c of the candidate pair, there is an added oxygen facing the pair's apical neighbor; the probability of which is $2w/(0.5 + w)$, and one minus this probability will thus enter as a necessary factor. The conjecture is that the added oxygen expands the thus formed octahedral coordination of the neighbor and this would trap the small pentacoordinated Fe^{3+} of the candidate pair. Rearranging the above terms, the $Fe^{2.5+}$ concentration can be written as

$$x_{Fe^{2.5+}} = 2(0.5 - w)\frac{0.5 - w}{0.5 + w}P_R. \quad (3)$$

The factor 2 accounts for the two members of the pair, and $P_R \approx 1$ is a generalization of a probability term in otherwise the same equation derived from different premises in Ref. [6], to allow for defects in the 100% probability of pairing. The R-subscript allows for a possible dependence on the rare-earth atom; fitting for $R =$ Eu gives $P_R = 0.92(3)$.

A corresponding decay of the valence-mixed states due to w is registered in the ^{151}Eu Mössbauer parameter internal field at the Eu nucleus that "sees" the presence of the valence-mixed iron owing to the ferromagnetic coupling associated with the valence-mixing iron pairs. This is illustrated by the curve in Fig. 9(a), drawn according to the rescaled probability function of Eq. (3).

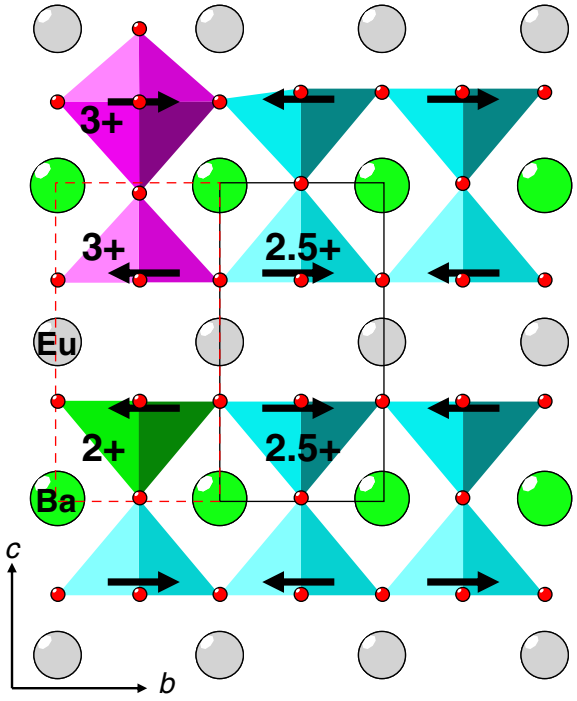

Fig. 11. Effect of oxygen nonstoichiometry (top left) on valence mixing of di- and trivalent iron via electron sharing in ferromagnetically coupled pairs across the Eu layer in $EuBaFe_2O_{5+w}$. Unit-cell frame of one of the mixing pairs is drawn in full line; of the nonmixing pair in dashed line.

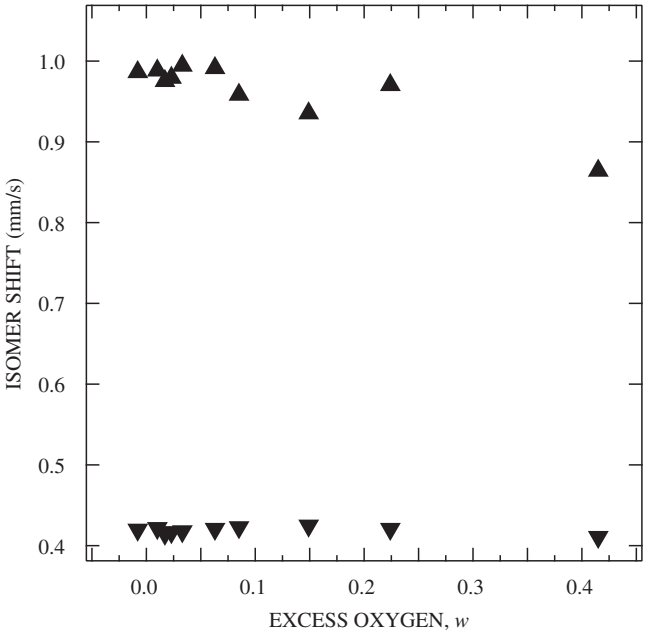

Fig. 12. Isomer shifts of the charge-ordered iron states at 77 K as a function of w.

4.2. Charge ordering under oxygen nonstoichiometry

The Mössbauer component $^{CN5}Fe^{2+}_{8\,T,\,CO}$ disappearing at T_V is one of the two charge-ordered states. If there is a direct parentage between this state and the valence-mixed state, the concentration of this component should be equal to $x_{Fe^{2.5+}}/2$ (Eq. (3); Fig. 10) for all nonstoichiometry levels w. Remarkably, it is not. The decrease in the concentration of the charge-ordered $^{CN5}Fe^{2+}_{8\,T,\,CO}$ can best be fitted as a linear function of w. It seems that the charge-ordered state is more robust against defects, i.e., many of the five-coordinated Fe^{2+} and Fe^{3+} atoms that order into chains will not participate in the valence-mixed pair formation when the charge-ordered state melts at T_V. Ideally, the intensity of $^{CN5}Fe^{2+}_{8\,T,\,CO}$ would be $0.5-w$ if all five-coordinated Fe species participated in charge ordering. Because there is another Fe^{2+} species present, denoted $^{CN5}Fe^{2+}_{25\,T}$ (Fig. 7), defects of the charge-ordered structure do exist, and the decay as a function of w is deeper than $0.5-w$, but not as deep as $x_{Fe^{2.5+}}/2$ of Eq. (3). Analogously, $^{CN5}Fe^{3+}_{50\,T}$ and $^{CN6}Fe^{3+}_{50\,T}$ represent defects in the trivalent part of the coherent charge-ordered structure.

Another important observation is that the isomer shift of the typically charge-ordered $^{CN5}Fe^{2+}_{8\,T,\,CO}$ changes very little as a function of w up to $w = 0.224$ (Fig. 12), even though it shows an increasing scatter owing to the decreasing concentration of this component. This supports the conclusion drawn from the thermodynamic data, viz., that for long-range charge ordering the oxygen nonstoichiometry does not affect the extent of the valence separation, but rather the amount of atoms that undergo the long-range charge ordering. These atoms then maintain the same practically integer valences two and three, independent of w. Only the short-range charge ordering concerns typically fractional valences.

The summary of how the charge ordering responds to increasing oxygen nonstoichiometry is given in Fig. 13. According to Ref. [3], the superstructure Bragg reflections of the coherent long-range charge order disappear from SXPD patterns at about $w = 0.03$. The remaining incoherent order of short chains of di- and trivalent iron along b exists up to $w \approx 0.25$, manifested by the enhanced orthorhombic distortion (over that associated with the magnetic order) as well as by the main Verwey-type transition being discontinuous in terms of both ΔV according to SXPD (Figs. 2 and 4) and ΔH by DSC (Fig. 5). The difference to the total concentration of the charge-ordered iron species accounted for by the Mössbauer spectroscopy represents the isolated, short-range, charge order (on a scale smaller than smallest domains of coherent X-ray diffraction), which persists up to at least $w \approx 0.4$ (Fig. 10). The residual iron states can be labeled charge-ordering defects.

Is there a fundamental difference between the defects of the charge-ordered structure and the defects of the valence-mixed structure? The answer to this question is no. All are regular Mössbauer states of iron, such as $^{CN5}Fe^{2+}_{25\,T}$, $^{CN5}Fe^{3+}_{50\,T}$ and $^{CN6}Fe^{3+}_{50\,T}$, with hyperfine parameters typical of the valence, oxygen coordination, etc., regardless of what the surrounding lattice is doing. Naturally, increasing

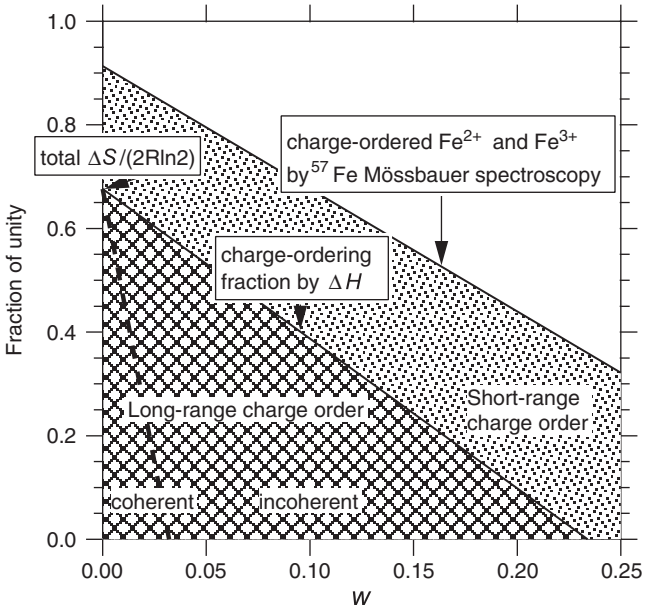

Fig. 13. Fractions of charge-ordering types as a function of w in polycrystalline $EuBaFe_2O_{5+w}$, as defined by ΔH of Verwey transition (Fig. 5) scaled to the fraction of observed and theoretical entropies, and as accounted for by Mössbauer spectroscopy (Fig. 10).

temperature will affect the internal fields and line-widths. Also the satellite component $^{CN5}Fe^{3+}_{satel,\,40\,T}$ observed only above T_V can be regarded as one caused by temperature. However, as follows from the above discussion, the concentration of these defects is not the same below and above T_V. Components $^{CN5}Fe^{2+}_{25\,T}$ and $^{CN5}Fe^{3+}_{50\,T}$ that did not participate in the valence mixing above T_V seem to lose intensity in favor of the charge-ordered structure below T_V. In the charge-ordered state, most of the five-coordinated defects are probably antisite atoms, i.e., Fe^{2+} occupying the site of Fe^{3+} and vice versa. Located at such an antisite, Fe^{2+} would neither have its typical geometry nor the strongly orthorhombically distorted polyhedron of the orbital-ordered divalent iron, something that explains the large differences in internal fields of the observed divalent iron states. Above T_V, the orthorhombically distorted coordination polyhedra of the charge-ordered divalent iron are no longer present, and Fe^{2+} adopts its regular internal field.

5. Conclusions

For $w \approx 0$, ^{57}Fe Mössbauer spectroscopy identifies one of the charge-ordered states in $EuBaFe_2O_{5+w}$ as trivalent. This implies that the second state is divalent. The isomer shift of this very typical charge-ordered Fe^{2+} is nearly independent of w up to the limit $w \approx 0.25$ of the long-range charge ordering seen by SXPD. This suggests that upon increasing w, the long-range charge-ordered iron states remain practically integer valences +2 and +3. In this nonstoichiometry range, ^{57}Fe Mössbauer spectroscopy registers a decreasing number of these charge-ordered states. Above the nonstoichiometry level of $w \approx 0.25$, the decrease in the number of charge-ordered states may be accompanied by their lower charge separation associated with a short-range order. A following picture can be summarized: the decrease in concentration of the long- and short-range charge-ordered iron couples is a linear function of w: the short-range order is likely to have a less complete charge separation. The long-range order is manifested by enhanced orthorhombic distortion and a discontinuous volume change at the onset of the ordering, which both disappear at the nonstoichiometry level of about $w = 0.25$. The latent heat of freezing into the long-range orbital- and charge-ordered state is a linear function of w and becomes zero close to $w = 0.25$, suggesting that each nonstoichiometric oxygen removes about one long-range charge-ordered unit cell (four iron atoms) from the long-range charge freezing. At low levels of w, a subset of the long-range ordered iron couples orders coherently across distances exceeding the minimum size of coherently diffracting domains, and this is manifested in a long-range charge-ordered superstructure observed by powder diffraction.

^{57}Fe Mössbauer spectroscopy registers a progressive removal of the valence-mixed iron states $Fe^{2.5+}$ as a function of w. This removal proceeds according to a probability scheme of mixing, imagined as a rapid cooperative [6] electron hopping along c between ferromagnetically coupled divalent and trivalent iron pairs distributed in a coulombically/sterically restricted pattern. It follows a formula practically identical with one derived [6] from somewhat different premises before the spin polarized coupling along c was established experimentally in Ref. [7]. Analogous information is registered by the ^{151}Eu Mössbauer spectroscopy, which shows that the increasing oxygen nonstoichiometry w decreases the magnetic field seen by the ^{151}Eu Mössbauer nucleus in direct correlation with the depletion of $Fe^{2.5+}$. This also proves the link between the ferromagnetic coupling and valence mixing. As a collateral, this result means that upon increasing w the magnetic order in $RBaFe_2O_{5+w}$ above the Verwey-type transition changes to the G-type.

Valence mixing and charge ordering are therefore two separate cooperative phenomena. According to ^{57}Fe and ^{151}Eu Mössbauer spectra, there is no direct parentage between the iron states above and below the Verwey-type transition, as their concentrations vary differently as a function of the oxygen nonstoichiometry w in $EuBaFe_2O_{5+w}$. The reason for this difference is that these two cooperative mechanisms are not the same: the thermally induced valence mixing is a probability driven electron sharing between ferromagnetically coupled Fe pairs along c, whereas the ordering concerns the doubly occupied d_{xz} orbitals of Fe^{2+}. These two mechanisms give practically the same degree of the cooperative effect for the ideally stoichiometric $RBaFe_2O_5$, but respond differently to perturbation with the added oxygens w.

Acknowledgments

Experimental assistance from the staff of the Swiss-Norwegian Beam Lines is gratefully acknowledged. Mr. N. Kaihovirta is acknowledged for his assistance with some of the Mössbauer measurements. J.L. acknowledges financial support from the Magnus Ehrnrooth foundation.

References

[1] P. Karen, K. Gustafsson, J. Lindén, J. Solid State Chem., (2006) in press, doi:10.1016/j.jssc.2006.09.21.
[2] P. Karen, P.M. Woodward, J. Mater. Chem. 9 (1999) 789–797.
[3] P. Karen, P.M. Woodward, P.N. Santosh, T. Vogt, P.W. Stephens, S. Pagola, J. Solid State Chem. 167 (2002) 480–493.
[4] P. Karen, J. Solid State Chem. 170 (2003) 9–23.
[5] P. Karen, J. Solid State Chem. 177 (2004) 281–292.
[6] J. Lindén, P. Karen, A. Kjekshus, J. Miettinen, T. Pietari, M. Karppinen, Phys. Rev. B 60 (1999) 15251–15260.
[7] P. Karen, P.M. Woodward, J. Lindén, T. Vogt, A. Studer, P. Fisher, Phys. Rev. B 64 (2001) 214405/1–214405/14.
[8] A.C. Larson, R.B. Von Dreele, General structure analysis system (GSAS), Los Alamos National Laboratory Report LAUR 86-748, 2000.
[9] P.M. Woodward, E. Suard, P. Karen, J. Am. Chem. Soc. 125 (2003) 8889–8899.